Journal of Molecular Modeling (2019) 25: 359
https://doi.org/10.1007/s00894-019-4235-9

ORIGINAL PAPER

Adsorption of carbon dioxide and ammonia in transition metal–doped boron nitride nanotubes

Kleuton Antunes Lopes Lima[1] · Wiliam Ferreira da Cunha[1] · Fábio Ferreira Monteiro[1] · Bernhard Georg Enders[2] · Marcelo Lopes Pereira Jr[1] · Luiz Antonio Ribeiro Jr[1]

Received: 8 February 2019 / Accepted: 15 October 2019 / Published online: 26 November 2019

Abstract

Density functional theory calculations were carried out to analyze the performance of single-walled boron nitride nanotubes (BNNT) doped with Ni, Pd, and Pt as a sensor of CO_2 and NH_3. Binding energies, equilibrium distances, charge transference, and molecular orbitals, as well as the density of states, are used to study the adsorption mechanism of the gas species on the surface of the nanotube. Our results suggest a considerable rise in the adsorption potential of BNNTs when the doping scheme is employed, as compared with adsorption in pristine nanotubes. Ni-doped nanotubes are observed to be the best candidates for adsorption of both carbon dioxide and ammonia.

Keywords Gas adsorption · Transition metal doping · BNNT · Carbon dioxide · Ammonia

Introduction

Since the early 2000s, several works dealing with carbon nanotubes (CNTs) and boron nitride nanotubes (BNNTs) as gas sensors have been published [1–7]. This interest from the scientific community is due to the favorable structural and electronic properties that these nanostructured materials present. In addition to those properties, interesting optical, magnetic, and thermodynamical characteristics allow for the potential use of such materials as energy storage devices [8–12] and even biosensors [13–15]. Some references suggested CNTs to be superior over BNNTs when it comes to energy storage applications [16, 17]. A particularly interesting study has achieved such a conclusion by investigating molecular hydrogen and methane adsorption in both kinds of single-wall nanotubes [18–20]. CNT presented the higher binding energy, thus suggesting that molecular species, in general, are expected to be more strongly bound to the nanotube surface. Although of crucial importance, the binding energy cannot be the sole property considered far as the adsorption potential of nanostructures is evaluated. Other electronic structure properties and structural stability should also be carefully studied since they impact the device's chemical and thermodynamic stabilities. Due to the early success CNTs have presented, the effort in investigating such properties in BNNTs has been considerably smaller. This fact presents a major drawback because BNNTs are known to be stable species that could potentially give rise to devices that operate in environments of extreme temperature and pH, for instance. Moreover, it is important to thoroughly investigate different properties of BNNTs using a correct doping scheme [21–23] because its relative performance disadvantage, when compared with CNTs, can be more than compensated while using a proper doping scheme.

The focus of the present work is to study the stability and electronic structure performance of BNNT nanotubes doped with Ni (nickel), Pd (palladium), and Pt (platinum) under the adsorption of CO_2 and NH_3. We focus our investigation on these gases due to their broad variety of applications and their proven harms to human health when higher concentrations are inhaled [24–28]. Especially CO_2,

This paper belongs to the Topical Collection VII Symposium on Electronic Structure and Molecular Dynamics – VII SeedMol

Electronic supplementary material The online version of this article (https://doi.org/10.1007/s00894-019-4235-9) contains supplementary material, which is available to authorized users.

✉ Luiz Antonio Ribeiro Jr
ribeirojr@unb.br

[1] Institute of Physics, University of Brasilia, Brasilia, 70919-970, Brazil

[2] Faculty of Planaltina, University of Brasilia, Brasilia, 73345-010, Brazil

Table 1 E_{ads}, Homo, Lumo, E_{gap}, and simulation time calculated using all methods and functionals available on materials studio for the case presented in Fig. 1b (CO2 adsorption)

Method	Functional	E_{ads} (eV)	Homo (eV)	Lumo (eV)	E_{gap} (eV)	Time (min)
LDA	PWC	− 0.2806	− 0.18169	− 0.112434	0.069	14.55
LDA	VWN	− 0,.810	− 0.181755	− 0.112480	0.069	14.91
GGA	PW91	− 0.2211	− 0.173381	− 0.102375	0.071	18.75
GGA	BP	− 0.1056	− 0.170089	− 0.098379	0.072	16.76
GGA	PBE	− 0.2150	− 0.172000	− 0.100000	0.071	16.02
GGA	BLYP	− 0.1053	− 0.163798	− 0.093072	0.071	17.40
GGA	BOP	− 0.0079	− 0.15945	− 0.087731	0.072	18.35
GGA	VWN-BP	− 0.1061	− 0.170153	− 0.984230	0.072	18.40
GGA	RPBE	− 0.0818	− 0.167564	− 0.095754	0.072	18.71
GGA	HCTH	− 0.0715	− 0.171473	− 0.098385	0.073	18.05
GGA	PBEsol	− 0.2145	− 0.173265	− 0.102795	0.070	18.50

which is a odorless and colorless gas, making it difficult to detect.

All the calculations were carried out in the scope of the density functional theory (DFT). Two main aspects are of particular importance to this approach. First, we briefly discuss the effects of the doping itself. Doping with Ni, Pd, and Pt is carried out either by substituting the boron or the nitrogen species. A comparison between these doping schemes is conducted together with that of the pristine nanotube. Second, and most important, we discuss the effects of the doped system with the adsorbent species. Our goal is to describe which is the best dopant in terms of adsorption energy equilibrium distance of the complex and charge transfer between the nanotube and either CO_2 or NH_3. The present work consists of a valuable contribution to the assessment of whether BNNT can be a realistic candidate for gas sensing or storage devices.

Methods

The electronic structure properties are calculated through the use of the DMol^3 module of the Materials Studio™ software suite [29–31] with BSSE correction by means of the counterpoise method. All the calculations are accomplished by considering the spin unrestricted generalized gradient approximation (GGA) with the PBE functional and DNP basis set [32]. The nuclei-valence electron interactions are represented by the inclusion of semicore DFT pseudopotentials [32]. According the benchmark presented in Tables 1 and 2, the GGA/PBE approach shows a good accuracy/time performance by estimating adsorption energies similar to the ones reported in the references [33–41], where this computational methodology was successfully used to study the gas adsorption mechanism on organic and inorganic nanotubes. The orbital cutting threshold is set to 4.0 Å and the optimization force to 0.01 eV. The K points in the Brillouin zone are considered in a (1, 1, 2) Monkhorst-Pack mesh [42]. A tetragonal unit cell of 25, 25, 6, 4 is set so that to avoid artificial interaction with the image of neighboring cells. In this work, we have simulated BNNT(6, 6) with 72 atoms as the adsorbant surface. Figure 1 presents the different schemes of gas attack considered in a pristine nanotube. The metal-doped nanostructures were attacked similarly by the gas species considering the carbon and the nitrogen atoms directly above the dopant metal. As the

Table 2 E_{ads}, Homo, Lumo, E_{gap}, and simulation time calculated using all methods and functionals available on materials studio for the case presented in Fig. 1c (NH3 adsorption)

Method	Functional	E_{ads} (eV)	Homo (eV)	Lumo (eV)	E_{gap} (eV)	Time (min)
LDA	PWC	− 1.6128	− 0.17001	− 0.101926	0.068	13.40
LDA	VWN	− 1.6136	− 0.17007	− 0.101971	0.068	13.60
GGA	PW91	− 1.1780	− 0.16214	− 0.091775	0.070	21.25
GGA	BP	− 1.0470	− 0.15883	− 0.087283	0.071	17.52
GGA	PBE	− 1.1780	− 0.15900	− 0.090000	0.069	15.90
GGA	BLYP	− 0.9385	− 0.15251	− 0.068974	0.069	18.33
GGA	BOP	− 0.8245	− 0.14816	− 0.077558	0.071	18.02
GGA	VWN-BP	− 1.0480	− 0.15889	− 0.087326	0.071	18.86
GGA	RPBE	− 0.9345	− 0.15663	− 0.085116	0.071	17.40
GGA	HCTH	− 0.8048	− 0.16031	− 0.088569	0.072	17.20
GGA	PBEsol	− 1.37261	− 0.16196	− 0.091778	0.070	22.01

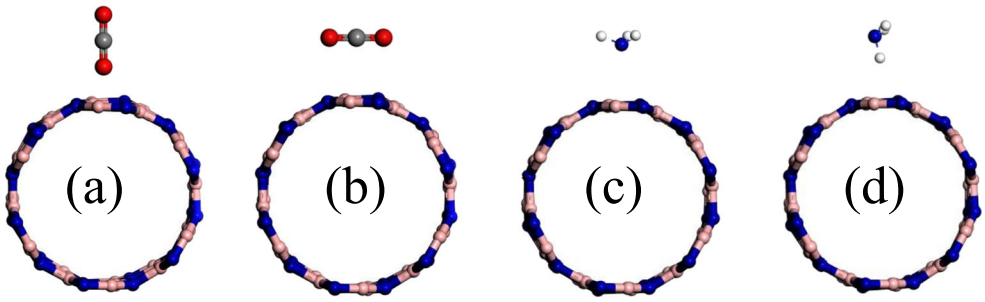

Fig. 1 Model BNNT/gas complexes studied here. Panels **a** and **b** and **c** and **d** illustrate, respectively, the considered positions of the CO_2 and NH_3 molecules concerning the BNNT. Note that these molecules are positioned on top of the dopant atom to maximize their interaction. In the color scheme, the atoms N and B are represented by the colors blue and pink, respectively

atomic radius of the metals is considerably larger than either boron and nitrogen, it is clear that the doped structure is deformed when compared with the pristine nanotube, with the dopant species outreaching outside the nanotube wall, as can be inferred from Fig. 2. Within this doping scheme, we intended to study how good is the possibility of capturing CO_2 or NH_3 above a critical distance to form the ligand complex. Importantly, the formation of ligand complexes involving these gases was already discussed [43].

The adsorption energy (E_{ads}) is computed as the difference between the electronic energy of the complex structure ($E_{complex}$) (after the adsorption process took place) and the sum of the potential energies of the isolated species (E_{BNNT} and E_{gas}) according to

$$E_{ads} = E_{complex} - E_{BNNT} - E_{gas}. \quad (1)$$

By employing a systematic variation of the distance between the gas specie and the nanotube, with corresponding single point calculations of the quantities in Eq. 1, potential energy curves (PECs) could be obtained. Other quantities such as frontier orbitals, density of states (DOS), Mulliken population, and intermolecular charge transference can be also evaluated. All those quantities, together with the bandgap energy E_{gap}, can be used to better understand fundamental electronic properties of the studied nanotubes.

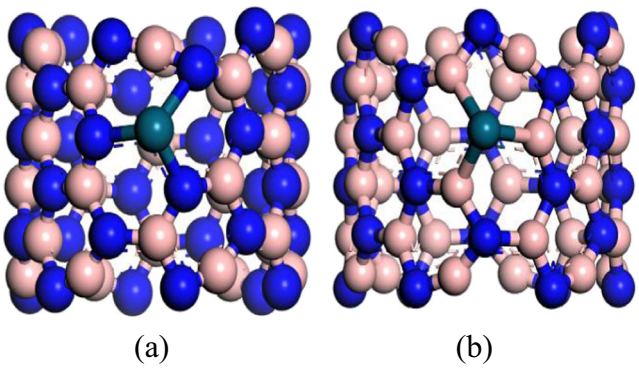

Fig. 2 Schematic representation of doped BNNTs. The dopant substitutes just one B atom in panel **a** and one N atom in panel **b** in the central region of the nanotube. The dopant is represented by green site

Results

We begin the analysis of the results presenting a summary table containing the structural and electronic characteristics of the different candidates to gas sensors (see Table 3). The idea is to isolate the best candidates in terms of site substitution, dopants, and adsorption direction (according to Fig. 1) so that the calculations above could be performed to the most promising cases.

In Table 3, R_e is the equilibrium distance of the complex, i.e., the point with the most negative energy, according to Eq. 1. E_{HOMO} corresponds to the energy of the highest occupied molecular orbital (HOMO) and E_{LUMO} to the energy of the lowest unoccupied molecular orbital (LUMO). E_{ads} and E_{gap} being the adsorption and bandgap energies, respectively, while Q_T stands for the charge transfer between structures. The notation adopted in the first column of the table begins with a letter corresponding to Fig. 1, which represents both the gas species and the direction of adsorption. A dash after the letter means the system is pristine, whereas the name of the atom represents the species substituted by the metal described in the second column.

In Table 3, we highlighted (in italic) the most promising systems as far as gas adsorption candidates are concerned. The goal is to carry out the remaining of the analysis in these particular systems.

For the adsorption of carbon dioxide, it was obtained that the attack configuration A was preferable when oxygen was directly towards the nickel dopant that replaced nitrogen from the nanotube. As for ammonia adsorption, it too yielded the most favorable adsorption with nickel substituting nitrogen, but this time when the gas approached the doped BNNT according to configuration C. One can

Table 3 Structural and electronic characteristics of candidates to gas sensors

Pos/dop	Structure	R_e (Å)	E_{HOMO} (eV)	E_{LUMO} (eV)	E_{ads} (eV)	E_{gap} (eV)	Q_T (e)
A/-	BNNT-CO2	2.98	− 0.246	− 0.092	− 0.063	0.153	− 0.004
A/B	BNNT@Ni-CO2	3.30	− 0.222	− 0.152	− 0.061	0.070	− 0.003
A/B	BNNT@Pd-CO2	2.99	− 0.213	− 0.184	− 0.062	0.028	− 0.001
A/B	BNNT@Pt-CO2	3.30	− 0.209	− 0.184	− 0.060	0.025	− 0.002
A/N	*BNNT@Ni-CO2*	2.20	− 0.172	− 0.100	*− 0.215*	0.071	− 0.003
A/N	BNNT@Pd-CO2	2.70	− 0.236	− 0.141	− 0.054	0.095	− 0.002
A/N	BNNT@Pt-CO2	3.00	− 0.245	− 0.141	− 0.071	0.104	− 0.001
B/-	BNNT-CO2	3.29	− 0.247	− 0.093	− 0.051	0.153	− 0.002
B/B	BNNT@Ni-CO2	3.70	− 0.224	− 0.154	− 0.020	0.070	− 0.001
B/B	BNNT@Pd-CO2	3.70	− 0.216	− 0.187	− 0.018	0.029	− 0.003
B/B	BNNT@Pt-CO2	3.61	− 0.212	− 0.187	− 0.004	0.024	0.007
B/N	BNNT@Ni-CO2	3.50	− 0.177	− 0.125	− 0.045	0.052	0.003
B/N	BNNT@Pd-CO2	3.50	− 0.241	− 0.145	− 0.033	0.096	0.002
B/N	BNNT@Pt-CO2	3.51	− 0.248	− 0.146	− 0.024	0.102	− 0.003
C/-	BNNT-NH3	2.70	− 0.237	− 0.089	− 0.168	0.148	0.003
C/B	BNNT@Ni-NH3	2.20	− 0.201	− 0.143	− 0.124	0.058	0.002
C/B	BNNT@Pd-NH3	2.50	− 0.202	− 0.173	− 0.132	0.029	0.001
C/B	BNNT@Pt-NH3	2.40	− 0.196	− 0.169	− 0.650	0.026	− 0.001
C/N	*BNNT@Ni-NH3*	2.10	− 0.159	− 0.090	*− 1.178*	0.069	0.005
C/N	BNNT@Pd-NH3	2.40	− 0.226	− 0.131	−0.620	0.095	0.003
C/N	BNNT@Pt-NH3	2.40	− 0.236	− 0.126	− 0.640	0.110	0.004
D/-	BNNT-NH3	2.40	− 0.225	− 0.093	− 0.051	0.131	0.004
D/B	BNNT@Ni-NH3	2.80	− 0.221	− 0.151	− 0.131	0.372	− 0.005
D/B	BNNT@Pd-NH3	3.30	− 0.210	− 0.185	− 0.128	0.029	− 0.004
D/B	BNNT@Pt-NH3	2.60	− 0.121	− 0.186	− 0.127	0.024	− 0.001
D/N	BNNT@Ni-NH3	2.20	− 0.176	− 0.121	− 0.130	0.055	− 0.003
D/N	BNNT@Pd-NH3	2.40	− 0.239	− 0.145	− 0.136	0.094	− 0.002
D/N	BNNT@Pt-NH3	2.60	− 0.232	− 0.146	− 0.135	0.086	− 0.001

The first column begins with a letter representing the gas species and the direction of adsorption according to Fig. 1. A dash after the first letter means the system is pristine, whereas the name of the atom represents the species substituted by the metal described in the second column. The remaining columns correspond to the parameters discussed in the "Results" section of the main text

note that, in general, the pristine BNNTs tend to present considerably higher adsorption energies than their doped counterparts. This fact is especially true for the nickel species which, indeed, is expected to be the most reactive of the studied metals.

Our conclusions are obtained mainly from the evaluation of adsorption energy. Overall, they can be summarized and presented as follows. Firstly, we obtained that nickel is the best dopant and its performance is especially favorable when substituting a nitrogen atom from the nanotube. Secondly, the adsorption process is facilitated when the most electronegative atom of the gas species is nearer the metal, a result that directly follows from the fact that metals are electron rich species.

Having these results in mind, we can now turn to the analysis of the PECs of the adsorption processes of both CO_2 and NH_3. Figure 3 a presents the PECs related to the adsorption process of the former according to configuration A of Fig. 1. Here, nitrogen is the substituted species on the nanotube whenever doping is carried out. The figure contains PECs of pristine (black), Pt-doped (blue), Pd-doped (red), and Ni-doped (green) BNNTs. One can see the difference between the depths of the wells, which can be as high as over an order of magnitude, reaching over 0.2 eV. The figure is a irrefutable proof of the importance of doping on the adsorption process in BNNTs. By doping BNNTs with nickel using substituting the lattice's nitrogen, a well deep enough that several vibrational levels would be borne. This fact could have a significant impact on the lifetime of the complex and, as a consequence, on its stability. Figure 3 b presents the comparison between the PECs of the NH_3 adsorption process by the different BNNTs. Once again,

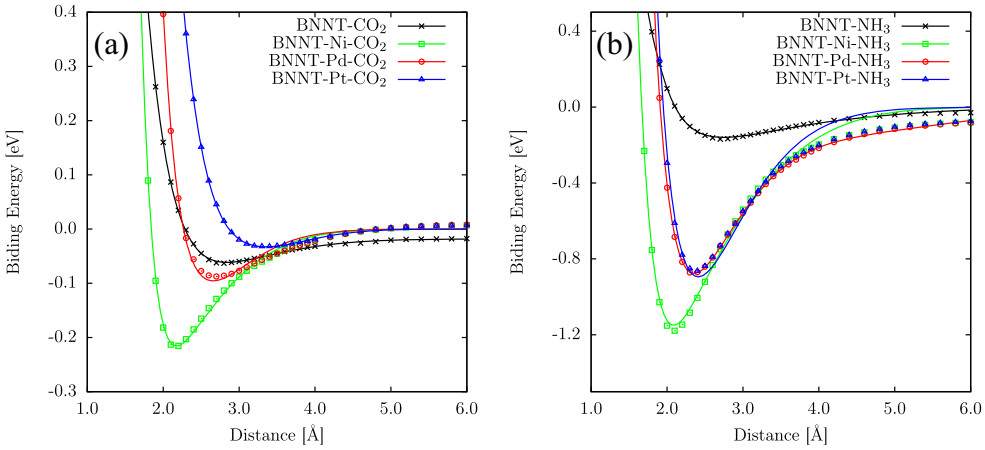

Fig. 3 Binding energy for nanotubes BNNT, BNNT@Ni, BNNT@Pd, and BNNT@Pt in the presence of **a** CO_2 and **b** NH_3

one can see the increase of the adsorption energy when the doping scheme is considered. In this case, the adsorption energy of the Ni-doped BNNT reaches 1.17 eV, the largest described in the present study.

Figure 4 compares the density of states between the pristine and Ni-doped BNNTs in their respective equilibrium distances. The differences of the pattern are remarkable thus suggesting that, indeed, the doping scheme profoundly affect the electronic structure of the system for both, NH_3 and CO_2. In particular, it is observed the lowering in the energy gap, manifested by the presence of states near 2.4 eV.

Figure 5 presents the frontier orbitals HOMO and LUMO. One can see that the presence of the dopant induces an even greater degree of localization of these orbitals around the adsorption site. Such properties can have influences over the electric features of a device such as the gas sensor. For instance, a diminishing of the energy gap contributes to a greater conductance of the system, thus allowing free charge carriers to move more efficiently through the lattice. This property can be used as a route to the detection mechanism of the gas species.

Other cases that have shown to be less prominent for CO_2 and NH_3 sensors, and which justify the choice made concerning the N-doped nanotubes with Ni used here, are presented in the supplementary material. For the sake of comparison, Table 3 presents several quantities for all complexes studied here (including the cases in which the potential energy curves and frontier orbitals are presented only in the supplemental material). Importantly, the results concerning pristine BNNTs show that they interact with the gases very weakly, corresponding to physical adsorption. When it comes to doped BNNTs, one can note that the geometrical deformations imposed by the atom substitution mechanism lead to changes in the electronic properties for the nanotubes. As depicted in Fig. 4, the calculated DOS shows how atomic substitution affects the electronic distribution of BNNTs. Adding a dopant atom to the BNNTs induces the appearance of some impurity states near the Fermi level, thus resulting in a gap decrease facilitating the charge transference among the levels. These new states also produce a change in the frontier orbital localization (as shown in Fig. 5) that enables the chemical adsorption between the BNNT region in the presence of a dopant

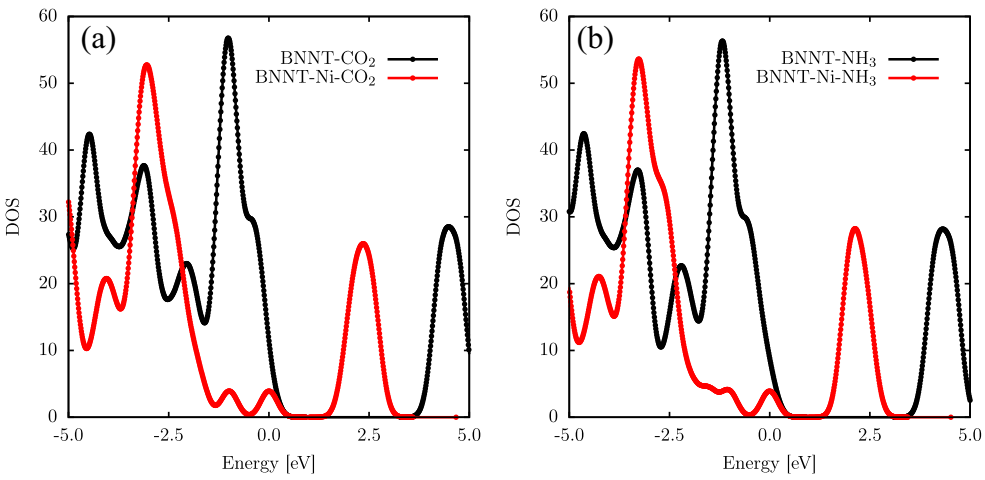

Fig. 4 Density of states for nanotubes BNNT (black lines) and BNNT@Ni (red lines) in the presence of **a** CO_2 and **b** NH_3

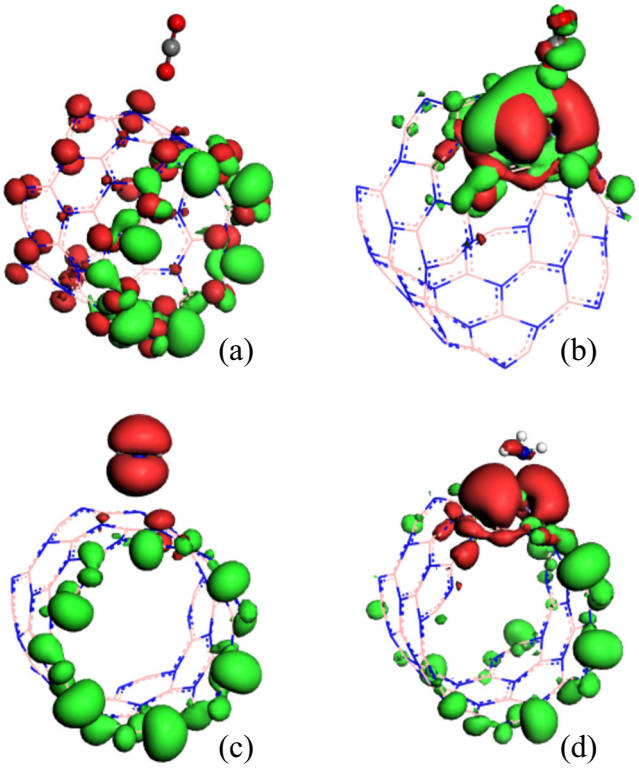

Fig. 5 HOMO-LUMO for CO_2 molecule in nanotube **a** BNNT and **b** BNNT@Ni, and the molecule of NH_3 in nanotube **c** BNNT and **d** BNNT@Ni

and the adsorbed gases. It is worthwhile to mention that chemical adsorption occurs for binding energies higher than 1 eV.

Conclusions

We have conducted a comprehensive study concerning the adsorption mechanism of carbon dioxide and ammonia in transition metal–doped BNNTs. We observed that the substitutional doping increases when the metal substitutes nitrogen on the adsorbant surface. Nickel was shown to be the dopant that increased the adsorption energy of either CO_2 or NH_3 the most. The present study shows that the viability of conceiving energy storage and gas sensing devices based on BNNTs requires specific doping schemes concerning both the nature of the site to be extracted from the system as well as the one to be included. Importantly, the Ni-doped CNTs were also employed to theoretically study the adsorption of CO_2 and NH_3 on nanostructures [44, 45]. These studies report that adsorption energies are − 1.93 for CNT@Ni-CO2 [44] and − 1.37 eV for CNT@Ni-NH3 [45]. Table 1 shows that the adsorption energies obtained here for CO_2 and NH_3 when it comes to nickel-doped BNNTs are − 0.21 eV and − 1.18 eV, respectively. In both cases, we can conclude that Ni-doped CNTs are more reactive structures than BNNTs analogs for the adsorption of CO_2 and NH_3. A possible reason for that is the shortest distance between the dopant and the CNT wall regarding the BNNT. This short distance allows the gas to interact with the atoms in the nanotube wall more strongly in the former case. Moreover, other studies have investigated the adsorption of CO_2 on pristine and doped BNTTs [37, 46, 47]. The calculated adsorption energies are about − 1.02 eV for doped BNNTs and − 0.16 eV for pristine structures. When it comes to NH_3 case, some works in the literature report the chemisorption mechanism, in pristine and doped structures, with energies varying from 0.45 to 2.5 eV [48, 49]. The values obtained here for the NH3 absorbed on BNNT@Ni structure, see Table 1, are similar to the ones reported in these studies.

Funding information The authors gratefully acknowledge the financial support from the Brazilian Research Councils CNPq and CAPES as well as CENAPAD-SP for providing the computational facilities. L.A.R.J. gratefully acknowledges the financial support from the Brazilian Research Council FAPDF grant 0193.001511/2017 as well as the Brazilian Ministry of Planning, Budget and Management (Grant DIPLA 005/2016). B.G.E., F.F.M., and W.F.C. also thank FAPDF for grants 0193.001556/2017, 0193.001234/2016, and 0193.001694/2017. L.A.R.J. gratefully acknowledge the financial support from CNPq grant 302236/2018.

References

1. Kong J, Franklin NR, Zhou C, Chapline MG, Peng S, Cho K, Dai H (2000) Science 287(5453):622
2. Schedin F, Geim A, Morozov S, Hill E, Blake P, Katsnelson M, Novoselov K (2007) Nat Mater 6(9):652
3. Collins PG, Bradley K, Ishigami M, Zettl dA (2000) Science 287(5459):1801
4. Gudiksen MS, Lauhon LJ, Wang J, Smith DC, Lieber CM (2002) Nature 415(6872):617
5. Li J, Lu Y, Ye Q, Cinke M, Han J, Meyyappan M (2003) Nano Lett 3(7):929
6. Wang R, Zhu R, Zhang D (2008) Chem Phys Lett 467(1-3):131
7. Han WQ, Zettl A (2003) J Am Chem Soc 125(8):2062
8. Kalay S, Yilmaz Z, Sen O, Emanet M, Kazanc E, Çulha M (2015) Beilstein J Nanotechnol 6(1):84
9. Ciofani G (2010) Expert Opin Drug Deliv 7(8):889
10. Salvetti A, Rossi L, Iacopetti P, Li X, Nitti S, Pellegrino T, Mattoli V, Golberg D, Ciofani G (2015) Nanomedicine 10(12):1911
11. Xue Y, Jiang B, Bourgeois L, Dai P, Mitome M, Zhang C, Yamaguchi M, Matveev A, Tang C, Bando Y et al (2015) Mater Des 88:451
12. Ciofani G, Danti S, D'Alessandro D, Ricotti L, Moscato S, Bertoni G, Falqui A, Berrettini S, Petrini M, Mattoli V et al (2010) ACS Nano 4(10):6267
13. Song X, Hu J, Zeng H (2013) J Mater Chem C 1(17):2952
14. Peyghan AA, Soltani A, Pahlevani AA, Kanani Y, Khajeh S (2013) Appl Surf Sci 270:25
15. Chopra NG, Luyken R, Cherrey K, Crespi VH, Cohen ML, Louie SG, Zettl A (1995) Science 269(5226):966
16. Froudakis GE (2011) Mater Today 14(7-8):324
17. Zhang F, Zhao P, Niu M, Maddy J (2016) Int J Hydrogen Energy 41(33):14535

18. Pradhan BK, Sumanasekera GU, Adu KW, Romero HE, Williams KA, Eklund PC (2002) Physica B: Condensed Matter 323(1-4):115
19. Tanaka H, El-Merraoui M, Steele W, Kaneko K (2002) Chem Phys Lett 352(5-6):334
20. Delavar M, Ghoreyshi A, Jahanshahi M, Nabian N (2014) J Exp Nanosci 9(3):310
21. Esrafili MD, Behzadi H (2013) Struct Chem 24(2):573
22. Deng ZY, Zhang JM, Xu KW (2015) Appl Surf Sci 347:485
23. Chen X, Dmuchowski CM, Park C, Fay CC, Ke C (2017) Sci Rep 7(1):11388
24. Fine GF, Cavanagh LM, Afonja A, Binions R (2010) Sensors 10(6):5469
25. Gomes F, Dmitriev V, Nascimento C (2014) J Microwaves Optoelectron Electromagn Appl 13(2):214
26. Tavangar Z, Hamadanian M, Basharnavaz H (2017) Chem Phys Lett 669:29
27. Habibi-Yangjeh A, Basharnavaz H (2018) Mol Phys 116(10):1320
28. Prajesh R, Goyal V, Bhargava J, Sharma A, Agarwal A (2017) Microsyst Technol 23(8):3027
29. Delley B (1990) J Chem Phys 92(1):508
30. Delley B (2000) J Chem Phys 113(18):7756
31. Andzelm J, Kölmel C, Klamt A (1995) J Chem Phys 103(21):9312
32. Delley B (2002) Phys Rev B 66:155125
33. Smith DGA, Patkowski K (2015) J Chem Phys C 119:4934
34. Li W, Li GQ, Lu XM, Ma JJ, Zeng PY, He QY, Wang YZ (2016) Chem Phys Lett 658:162
35. Li W, Ma JJ, Liu P, Pan ZL, He QY (2015) App Surf Sci 335:17
36. Li W, Lu XM, Li GQ, Ma JJ, Zeng PY, Chen JF, Pan ZL, He QY (2016) App Surf Sci 364:560
37. Mahdavifar Z, Abbasi N, Shakerzadeh E (2013) Sensors Actuat 185:512
38. Zhang Y, Liu Y, Meng Z, Ning C, Xiao C, Deng K, Jena P, Lu R (2018) Phys Chem Chem Phys 20:17599
39. Dandeliya S, Srivastava A (2015) 2015 IEEE international symposium on nanoelectronic and information systems, pp 268–271
40. Chermahini AN, Teimouri A (2017) J Chin Chem Soc 64:250
41. Santucci S, Picozzi S, Gregorio FD, Lozzi L, Cantalini C, Valentini L, Kenny JM, Delley B (2003) J Chem Phys 119:10904
42. Monkhorst HJ, Pack JD (1976) Phys Rev B 13:5188
43. Paura ENC, da Cunha WF, Roncaratti LF, Martins JBL, e Silva GM, Gargano R (2015) RSC Adv 5:27412
44. Nguyen TTH, Le VK, Minh CL, Nguyen NH (2017) Comp Theo Chem 1100:46
45. Tontapha S, Wanno B, Amorkitabamrung V, Sang-Aroon W (2015) Mah Int J Eng Tech 1:16
46. Paura ENC, da Cunha WF, de Oliveira Neto PH, e Silva GM, Martins JBL, Gargano R (2013) J Phys Chem A 117:2854
47. Paura ENC, da Cunha WF, Martins JBL, e Silva GM, Roncaratti LF, Gargano R (2014) RSC Adv 4:28249
48. Ahmadi A, Beheshtian J, Hadipour NL (2011) Struc Chem 22:183
49. Wu X, An W, Zeng XC (2006) J Amer Chem Soc 128:12001